

Clonal Selection Based Artificial Immune System for Generalized Pattern Recognition

Terry Huntsberger, Senior Member, IEEE
Autonomous Systems Division
NASA Jet Propulsion Laboratory,
California Institute of Technology
Pasadena, CA, 91109 USA
Terry.Huntsberger@jpl.nasa.gov

Abstract— The last two decades has seen a rapid increase in the application of AIS (Artificial Immune Systems) modeled after the human immune system to a wide range of areas including network intrusion detection, job shop scheduling, classification, pattern recognition, and robot control. JPL (Jet Propulsion Laboratory) has developed an integrated pattern recognition/classification system called AISLE (Artificial Immune System for Learning and Exploration) based on biologically inspired models of B-cell dynamics in the immune system. When used for unsupervised or supervised classification, the method scales linearly with the number of dimensions, has performance that is relatively independent of the total size of the dataset, and has been shown to perform as well as traditional clustering methods. When used for pattern recognition, the method efficiently isolates the appropriate matches in the data set. The paper presents the underlying structure of AISLE and the results from a number of experimental studies.

Keywords—artificial immune system; pattern recognition; classification

I. INTRODUCTION

Artificial Immune Systems (AIS) are loosely modeled after the human immune system. Without going too deeply into the details, the human immune system basically consists of a collection of lymphocyte cells that are produced in the thymus (T-cells) and in the bone marrow (B-cells). The functions of the T-cells include the regulation of other cells' actions and direct attacks on the host infected cells. The main functions of the B-cells include the production and secretion of antibodies as a response to antigens such as bacteria, viruses and tumor cells. Bindings between the antibody and the antigen occur at epitopic sites on the surface of the antigen where there are "shape" matches. The physical shape and chemical affinity of each antibody makes it specific to a very narrow range of antigens, so they act as efficient pattern recognition engines.

The dynamics of the immune system reaction to an antigen intrusion lends itself well to AIS methods for a wide range of applications including network intrusion detection [1], job shop scheduling [2], pattern recognition [3, 4, 5], and robot control [6, 7]. There have also been a number of studies into use of AIS for image classification [8, 9, 10, 11]. These types of

problems are characterized by a large set of data elements (size of images) that the system must be able to handle in an efficient manner. A commonly used short cut is to map the image data elements into a binary representation that leads to fast comparisons between data elements and the existing lymphopathic cells in the system. A recent comprehensive bibliography can be found in [12], and there are also many surveys of the field [13, 14, 15, 16, 17].

AIS approaches can be generally broken into two classes: population based and network based. The population-based algorithms rely on the dynamics of populations of individual immune-like cells. Examples of population-based systems include self/non-self [18, 19], immune libraries [20], clonal selection [21, 22], and hybrids [23]. The network based-algorithms are derived from the Immune Network Theory of Jerne [24], and rely on the interactions between networks of immune-like cells. Examples of network-based systems include case-base reasoning system for classification [25], anomaly detection [26], unsupervised learning [27, 28, 29], and continuous learning [30].

JPL has developed an integrated learning/pattern recognition/classification system called AISLE (Artificial Immune System for Learning and Exploration) based on models of B-cell dynamics found in human immune systems. It is a hybrid of a population-based and a network-based system, where the network interactions are modeled through cross-linking between B-cell populations, and clonal selection is accomplished by solving a differential equation of the B-cell population dynamics.

The next section discusses the B-cells dynamics model and gives some examples of its behavior when "exposed" to multi-

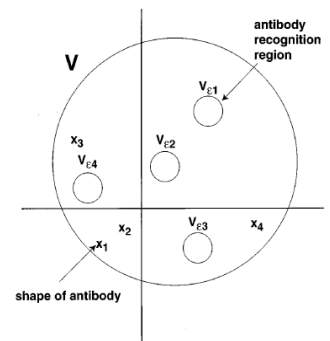


Figure 1. Illustration of shape space where any antibody shape only matches epitopes within a volume V [31].

This work was carried out at the Jet Propulsion Laboratory, California Institute of Technology, under a contract with the National Aeronautics and Space Administration.

© 2011 California Institute of Technology. Government sponsorship acknowledged.

dimensional patterns. The next section describes three experimental studies using a standard machine learning dataset, star tracking, and a satellite hyperspectral sensing dataset. The final section is a summary and description of future directions.

II. B-CELLS DYNAMICS MODEL

Since the B-cell dynamics are used for the system described in this paper, the following discussion will concentrate on them. An abstract model of binding in which receptors and antigens are considered as points in a ‘shape space’ (shown in Figure 1) with affinity measured as a function of the distance between such points [31] is a convenient computational AIS model, although there is still controversy surrounding the biological basis [32]. The shape space is equivalent to the feature space used for pattern recognition. The distance between shape space points is typically measured using Euclidean, Hamming, or Manhattan measures. The stronger the affinity between receptor and antigen, the greater the response of the B-cells. Population growth is directly dependent, and is coupled with somatic hypermutation [33] which is inversely dependent, on the strength of this interaction. Somatic hypermutation is the process whereby poorly matching clonal populations are selectively mutated to provide wider coverage of the shape space. In addition, there is a cross-linking between populations of B-cell receptors.

An expression has been derived for the population dynamics of the B-cells that incorporates all of these

$$\frac{\partial b_i}{\partial t} = s + b_i \left[\frac{p\theta}{\theta + b_i} f(h_i, h_i') + K_{iA} - d \right] \quad (1)$$

characteristics [34]. The population of the B-cells is governed by the differential equation:

which is a modification of the original dynamics equation [34] that restores a term for the direct affinity of the cell for the incoming antigen [35]. In this expression, b_i is the number of cells of clone i , s is the rate of influx of newly generated cells, p is the maximal growth rate, θ is the growth clone-size threshold, $f(h_i, h_i')$ is the cell activation function, K_{iA} is the affinity that the cell i has for the incoming pattern, and d is the death rate. The cell activation function is dependent on the binding between the individual B-cell populations in the network. Cells with higher affinity to the incoming pattern will clone themselves (with or without mutation) faster than those that are not as good a match. The cell activation function is defined as:

$$f(h_i, h_i') = \frac{(1 + 4w) h_i'}{w(1 + h_i)^2 + h_i'} \quad (2)$$

where the binding field is:

$$h_i = \sum_j K_{ij} b_j \quad (3)$$

the cross-linking field is:

1. Randomly initialize the starting B-cell population in the case of unsupervised learning, or load the Memory Cell population in the case of classification/recall.
2. Present the Input Data to AISLE one data element at a time.
3. Perform shape space culling of the initial population based on the specified distance metric (Euclidean, Hamming, Manhattan).
4. Iterate Equation (1) until there is only a single B-cell population left or a fixed number of generations have occurred. This step can include somatic hyper-mutations or can just use the population dynamics of (1). In the case of allowing somatic hyper-mutations, these new B-cell clones are added to the population for subsequent processing of new data elements.
5. Perform Steps 2-4 until all of the data elements have been processed. All of the B-cell population and additional hyper-mutated clones (if enabled) from Step 1 are included in the processing each time, and a Memory Cell population is maintained based on the surviving B-cells after the exposure of each data element.

Figure 2. AISLE algorithm.

$$h_i' = \sum_j K_{ij}^{\eta+1} b_j \quad (4)$$

and the affinity is:

$$K_{ij} = e^{-\frac{|x_i - x_j|^2}{2\sigma^2}} \quad (5)$$

The exponent η in the cross-linking term (4) controls the width of the cross-linking field. The distance between the shapes x_i and x_j in (5) is measured using a representative metric, and σ is the standard deviation. There is some evidence that the affinity (5) is only approximated by a Gaussian in the actual biological systems [36] with the width and height dependent on equilibrium constants, but for the purposes of the AIS the symmetrical Gaussian will serve the purpose.

In addition to the clonal population dynamics given in expression (1) through (5), there is a longer duration process called Memory Cell generation for the most responsive B-cells found during the exposure to the incoming patterns. The Memory Cell population persists for a longer duration and reacts much more quickly to new patterns [37]. This type of

behavior is in some sense equivalent to the training phase of a traditional learning system.

The AISLE system algorithm is shown in Figure 2. For unsupervised learning, a variable number of B-cell populations are randomly initialized and each input pattern is presented to the system. Equation (1) is used to process each data element, with a Memory Cell population being maintained based on the surviving populations after each data presentation. As each generation of B-cells is modified based on (1), cell death very quickly leads to a decreased number of interactions. The final surviving B-cell is put into the Memory Cell population to be included in the next exposure of the system.

III. EXPERIMENTAL STUDIES

A series of three experiments were run in order to test the learning and pattern recognition capabilities of AISLE. The first study uses the Fisher Iris dataset, the second study uses information derived from the Hipparcos star catalog, and the third study uses 18 dimensional spectral data acquired by the MODIS satellite. In all experiments, b_i , the number of cells of clone i , was initially set to 100 for all i , the influx rate s was set to 0.0001, the maximal growth rate p was set to 8, the growth clone-size threshold θ was set to 75, the activation w was set to 0.1, weight σ in the affinity function (5) was set to 5.0, the exponent η in the cross-linking term (4) was set to 1.0, and the death rate d was set to 1. All updates of (1) were done using a Euler rule with a time step of 1.0, the death decision for any population i was set to 50.0, and a maximal number of generations for each B-cell clone set to 5000.

A. First Study

The first study used one of the most studied classification testbeds, the Fisher Iris dataset [38], a collection of 150 flower samples with the four variables of sepal length, sepal width, petal length, and petal width. The dataset has been broken into the three classes Setosa, Versicolor, and Virginica based on visual analysis of the samples. The three classes are not linearly separable, with mixing between Versicolor and Virginica. This study was used to demonstrate the unsupervised learning capabilities of AISLE using a single exposure of 75 randomly selected members of the dataset to the system. The Memory Cell population in the worst case would have 75 elements corresponding to an element for each member of the data subset. There were 50 trials performed using different starting subsets. Memory Cell population members were labeled with the class of the input sample that triggered the B-cell population in order to determine the classification accuracy of the system. The final Memory Cell population had 11 members after the single exposure of the data subset to AISLE.

The full dataset was presented to AISLE in recall mode using only the Memory Cell population to determine how well the system learned. The overall classification accuracy was 94.67%, with a 100% identification of Setosa, eight misclassified Versicolor as Virginica, and one misclassified Virginica as Versicolor. This classification performance is equivalent to that of a backpropagation network with one hidden layer of 19 nodes or the SVM algorithm, and only slightly less than the 96% accuracy obtained by a recursive

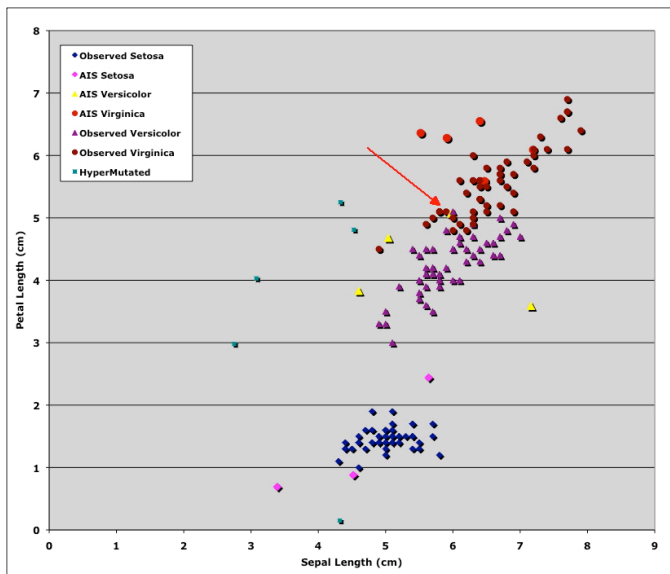


Figure 3. Experimental results from the exposure of the Fisher Iris dataset to AISLE in a single unsupervised pass. The B-cell populations that survived each exposure were put into a Memory Cell population. There were 11 Memory Cells left after the exposure of the full dataset. These are shown as the magenta diamonds (Setosa), yellow triangles (Versicolor), and red circles (Virginica).

partitioning algorithm [39]. AISLE achieves this level of classification performance with an order of magnitude better than that of the backpropagation network in terms of computational cycles. A plot of the AISLE results is shown in Figure 3. The plot shows petal length versus sepal length, and the clear delineation of Setosa is evident. Members of the Memory Cell population are also shown on the plot, and the source of the misidentification of Versicolor and Virginica lies in the Memory Cell (shown with arrow) within the boundary zone between the two classes. Also shown are members of the somatic hypermutated population that did not persist through the initial presentation of the dataset due to low final populations.

B. Second Study

The second study uses data from a subset of the Hipparcos star catalog. This catalog contains 118,218 stars that were observed by the European Space Agency's Hipparcos Satellite, operational from late 1989 to 1993. The Hipparcos catalog data is purely based on observations performed in space, except for the global orientation of its reference frame that was adjusted to the existing system by a variety of mainly ground-based techniques. By international agreement the catalog is the standard reference for optical astrometry. The subset of the catalog used for this study contained 2854 stars all with an apparent brightness magnitude cutoff of 5.5 found within 33 parsecs of Earth. This type of dataset would be used for star catalogs onboard a satellite to determine overall attitude within a global reference frame based on observed stars. An example of sample images taken at two instants in time is shown in Figure 4 for a simulated yaw maneuver of 1.41 degrees. The sizes of the stars indicate relative magnitudes.

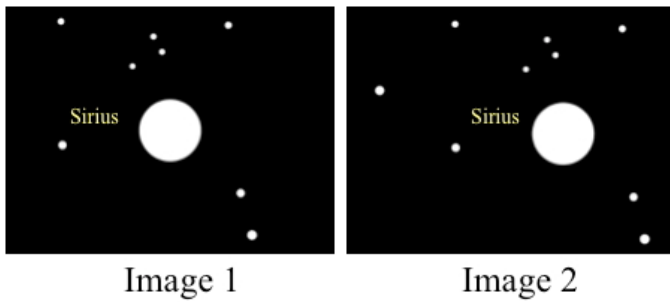


Figure 4. Two frames from a simulated satellite star tracking system. The placement of stars is based on the Hipparcos catalog entries. A yaw maneuver of 1.41 degrees is the position change from Image 1 on the left to Image 2 on the right. The relative sizes of the circles are correlated with the apparent magnitude taken from the catalog

Usually, only the star magnitudes are used as an index into the catalog to determine position. The relative positions of the stars are as important for matching, since the catalog has a large number of members and there will be a lot of mismatches if based on apparent magnitude alone. Characterizing the relative positions of the stars has to be done in such a way that is rotationally invariant, because the satellite can be in any orientation. For this reason, a composite vector was automatically built with sets of star triangles generated from the catalog using a Delaunay decomposition [40] of the data. An example of the Delaunay decomposition is shown in Figure 5, where 13 triangles capture the entire content of the image. The rotationally invariant representation is built using six variables derived from the triangles: the three first order shape moments [41] and the three star magnitudes on the corners of each triangle.

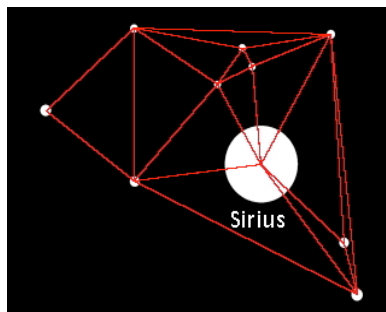


Figure 5. Delaunay decomposition of Image 2 from Figure 5. There are 13 triangles generated that serve as the basis for building a feature vector.

The first image in the sequence is fed into AISLE using a master Memory Cell population built from vectors derived from the Hipparcos catalog. The subset of matched vectors are then used as a new Memory Cell population for analysis of the next image. The number of surviving populations gives an indication of the degree of match, and any other triangle magnitude/moment vectors that are generated (epitopes) are the new stars that have entered the field of view of the satellite sensor due to the rotation. Figure 6 shows a plot of the final populations and the number of generations (iterations) for each of the triangle magnitude/moment vectors. The recognized vectors are characterized by relatively rapid convergence with convergence in all cases in about 300 msec making the algorithm capable of running in real time on a conventional processor or spacecraft. The matched triangle

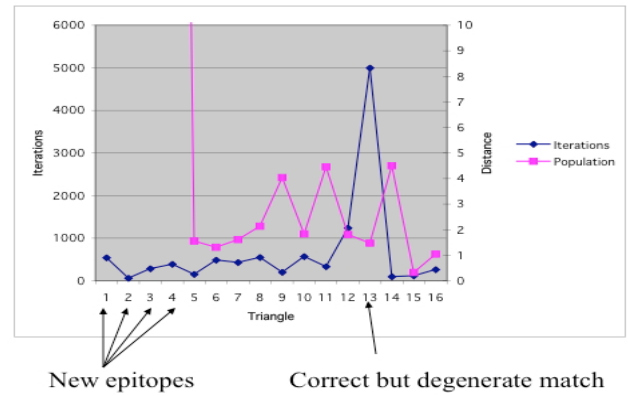


Figure 6. Plot of the number of generations (iterations) of AISLE required for each of the triangles in Figure 6 using the Memory Cell populations derived from the first frame of the sequence. The populations are consistent with the correct matches.

magnitude/moment vectors are shown in Figure 7, where the newly found vectors are labeled as epitopes.

C. Third Study

The final study demonstrates the clustering performance of AISLE. Usually, the object of a cluster analysis of remotely sensed data is to determine the dominant “classes” in the dataset for identification of land/water types. The dataset used in the study is from a hyper-spectral (18 bands) MODIS satellite feed (shown in Figure 8) taken over the Marqueses Islands (140°W, 10°S) located in French Polynesia in the Pacific Ocean. There are heavy currents that tend to obscure the boundaries between land and sea areas (especially at the relatively coarse 36 km cell size resolution of the data). Each of the 64,000 18-dimensional vectors corresponding to a location in the images was fed into AISLE much the same way as the first study – any surviving B-cell population is added to the Memory Cell population and used for the exposure of the next data item. The final Memory Cell population had 14 members that would correspond to 14 traditional classes for an unsupervised clustering algorithm. The study zone and output of the system is shown in Figure 9, where color coding is used in the inset to indicate the classes. The Marqueses Islands and Tuamotu Archipelago (circled in red) have been clearly extracted (yellow-tan labeled cells).

IV. SUMMARY AND CONCLUSIONS

This paper has presented AISLE, a clonal B-cell population based AIS that demonstrated generalized learning and pattern recognition capabilities. The Memory Cell populations are automatically generated by AISLE during the presentation of patterns. AISLE scales well for higher dimensional data, and all of the experimental studies were done using an ordinary MacBook Pro laptop (2.66 GHz Intel Core i7 CPU, 4 GB 1067 MHz RAM). The computational complexity of the system was kept under control using shape space culling of the initial large number of B-cell populations. The experimental studies demonstrated the unsupervised learning capabilities with a 94.67% accuracy on recall for the Fisher Iris dataset after only

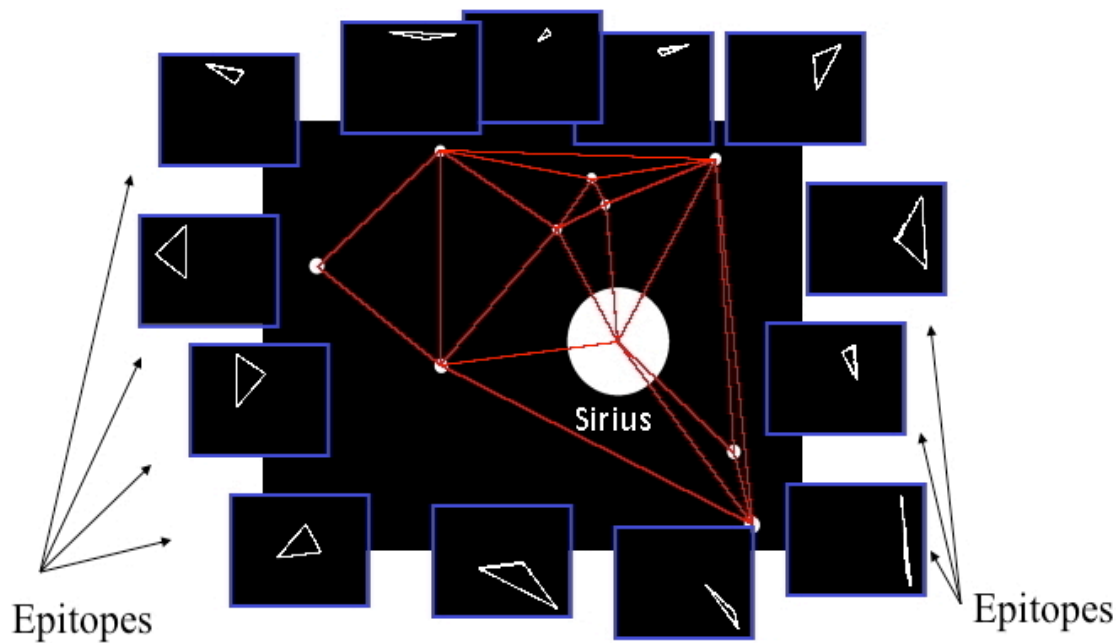


Figure 7. Matched triangle magnitude/moment vectors from the Memory Cell population derived from the first frame of the sequence for the second frame of the sequence. A total of 7 new triangle magnitude/moment vectors (epitopes) were found and these are then matched to the Master Hipparcos Star catalog to determine the movement of the satellite in between frames.

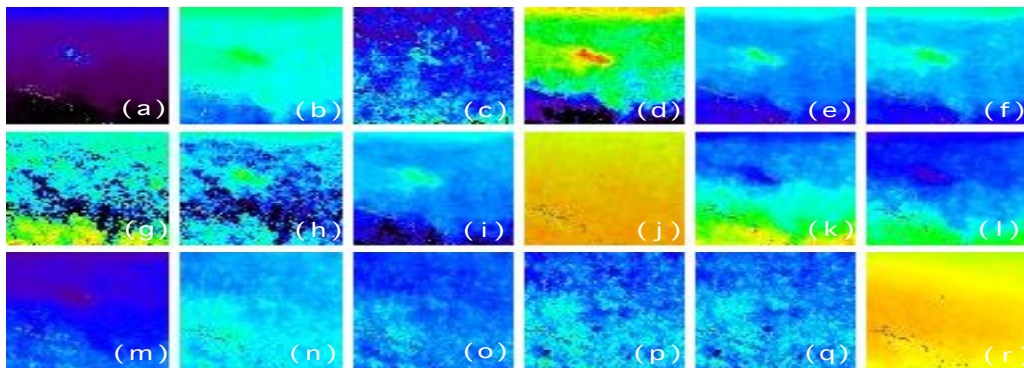


Figure 8. MODIS ocean data from Dec 1, 2000 for 18 bands of a study region centered on Marquesas Islands at 36km spatial resolution: (a) Gelbstoff absorption coefficient at 400 nm; (b) instantaneous absorbed radiation by phytoplankton for fluorescence; (c) calcite concentration; (d) phytoplankton absorption coefficient at 675 nm; (e) chlorophyll-a concentration (SeaWiFS analog - OC3M); (f) chlorophyll-a concentration (semianalytic); (g) chlorophyll fluorescence efficiency; (h) chlorophyll fluorescence line height; (i) chlorophyll-a concentration (HPLC, empirical); (j) instantaneous photosynthetically available radiation; (k-q) normalized water-leaving radiance at 412, 433, 488, 531, 551, 667, 678 nm; (r) sea surface temperature (11/12 micrometer).

a single pass, pattern recognition capabilities on a star tracking dataset with matching of common features in a sequence, and clustering capabilities on an 18 dimensional feature vector.

Current research directions include investigation of using GPU (Graphics Processing Units) on the laptop for better performance, developing a resolving strategy for degenerate matches (using other matches within the image), parallel processing, and developing an affinity based method for somatic hyper-mutations. Also underway are studies investigating the scalability of AISLE for larger hyperspectral datasets (256 bands) in an effort to determine what are the dominant bands that are useful for discrimination.

ACKNOWLEDGMENT

The author would like to thank JPL for providing the funding for this research under the Research and Technology Development Program.

REFERENCES

- [1] S. A. Hofmeyr and S. Forrest, "Immunity by design: An artificial immune system," Proc. Genetic and Evolutionary Computation Conference, Orlando, FL, pp. 1289–1296, July 13-17, 1999.
- [2] C. A. C. Coello, D. C. Rivera, and N. C. Cortes, "Use of an Artificial Immune System for Job Shop Scheduling," Proc. Second International Conference on Artificial Immune Systems (ICARIS), September 1-3, 2003, Napier University, Edinburgh, UK.

[3] J. H. Carter, "The immune system as a model for classification and pattern recognition," *Journal of the American Informatics Association*, vol. 7, no. 1, pp. 28-41, 2000.

[4] J. A. White and S. M. Garrett, "Improved pattern recognition with artificial clonal selection," *Artificial Immune Systems, Lecture Notes in Computer Science*, vol. 2787, pp. 181-193, 2003.

[5] A. Watkins, J. Timmis, and L. Boggess, "Artificial Immune Recognition System (AIRS): An Immune Inspired Supervised Machine Learning Algorithm," *Genetic Programming and Evolvable Machines*, vol. 5, no. 1, March 2004.

[6] N. Mitsumoto, T. Fukuda, and T. Idogaki, "Self-organising multiple robotic system," *Proc. IEEE International Conference on Robotics and Automation (ICRA96)*, Minneapolis, USA: IEEE, 1996, pp. 1614-1619.

[7] D.-W. Lee, H.-B. Jun, and K.-B. Sim, "Artificial immune system for realisation of co-operative strategies and group behaviour in collective autonomous mobile robots," *Proc. Fourth International Symposium on Artificial Life and Robotics*. AAAI, 1999, pp. 232-235.

[8] D. McCoy and V. Devarajan, "Artificial Immune Systems for Aerial Image Segmentation," *Proc. IEEE International Conference on Systems, Man, and Cybernetics*, Orlando, Florida, pp. 867-872, October 1997.

[9] K. Lackner and G. Cserey, "GPU Powered Artificial Immune System for Visual Applications," *Proc. IEEE International Symposium on Circuits and Systems*, Taipei, Taiwan, pp. 1221-1224, May 2009.

[10] G. Cserey, W. Porod, and T. Roska, "An Artificial Immune System Based Visual Analysis Model and Its Real-Time Terrain Surveillance Application," *Lecture Notes in Computer Science*, vol. 3239, Springer-Verlag, Berlin, pp. 250-262, 2004.

[11] S. Satyanath and F. Sahin, "Artificial Immune Systems Approach to a Real Time Color Image Classification Problem," *Proceedings IEEE International Conference on Systems, Man, and Cybernetics*, vol. 4, pp.2285-2290, 2001.

[12] D. Dasgupta, "Artificial Immune Systems: A Bibliography," Technical Report CS-07-004, Vers. 5.8, Computer Science Department, University of Memphis, December, 2008.

[13] A. Perelson and G. Weisbuch, "Immunology for physicists," *Reviews of Modern Physics*, vol. 69, no. 4, pp. 1219-1267, 1997.

[14] D. Dasgupta, "An overview of artificial immune systems and their applications," Chap. 1 in *Artificial Immune Systems and Their Applications*, Springer-Verlag, pp. 1-21, 1999.

[15] L. N. de Castro and F. J. Von Zuben, *Artificial Immune Systems: Part I—Basic Theory and Applications*, Technical Report DCA-RT 01/99, School of Computing and Electrical Engineering, State Univ. of Campinas, Brazil, 1999.

[16] L. N. de Castro and F. J. Von Zuben, *Artificial Immune Systems: Part II—A Survey of Applications*, Technical Report DCA-RT 01/00, School of Computing and Electrical Engineering, State Univ. of Campinas, Brazil, 2000.

[17] F. Liu, Q. Wang, and X. Gao, "Survey of Artificial Immune System," *Proc. 1st International Symposium Systems and Control in Aerospace and Astronautics (ISSCAA 2006)*, 19-21 Jan. 2006, pp. 985-991, 2006.

[18] S. Forrest, A. Perelson, L. Allen, and R. Cherukuri, "Self-Nonself Discrimination in a Computer," in *Proceedings of the 1994 IEEE Symposium on Research in Security and Privacy*, Los Alamitos, 1994.

[19] D. Dasgupta and S. Forrest, "An anomaly detection algorithm inspired by the immune system," in *Artificial Immune Systems and Their Applications* (Ed. D. Dasgupta), Springer, Berlin, pp. 262-277, 1998.

[20] R. Hightower, S. Forrest, and A. S. Perelson, "The evolution of emergent organization in immune system gene libraries," *Proc. Sixth International Conference on Genetic Algorithms*, Morgan Kaufmann, San Francisco, CA, pp. 344-350, 1995.

[21] F. Burnet, *The Clonal Selection Theory of Acquired Immunity*, Cambridge University Press, 1959.

[22] L. N. de Castro and F. von Zuben, "Learning and optimization using the clonal selection principle," *IEEE Transactions on Evolutionary Computation*, vol. 6, no. 3, pp. 239-251, June 2002.

[23] J. W. Kim, "Integrating artificial immune algorithms for intrusion detection," Ph.D. dissertation, Department of Computer Science, University College London, 2002.

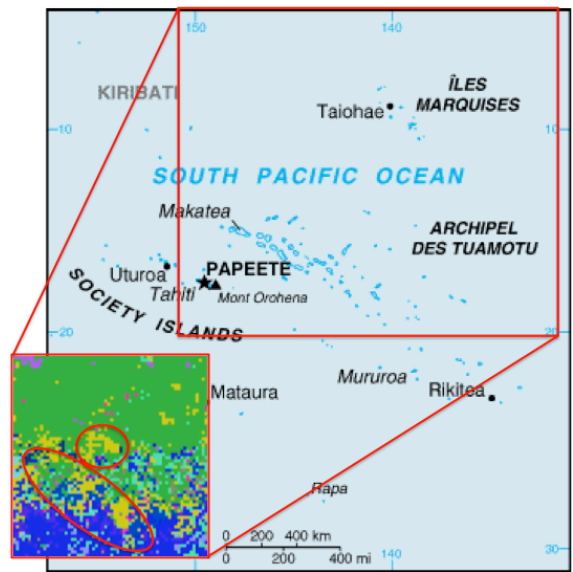


Figure 9. Study zone for Third Study centered on the Marquesas Islands. Inset shows the color coded output of AISLE operating in an unsupervised clustering mode. The Marquesas Islands and Tuamotu Archipelago and circled in red.

[24] N. K. Jerne, "Towards a network theory of the immune system," *Annals of Immunology (Inst. Pasteur)*, vol. 125C, pp. 373-389, 1974.

[25] J. Hunt and A. Fellows, "Introducing an immune response into a CBR system for data mining," *Research and Development in Expert Systems XIII*, Springer-Verlag, pp. 35-42, 1996.

[26] H. Aisu and H. Mizutani, "Immunity-based learning—integration of distributed search and constraint relaxation," in *International Workshop on the Immunity-Based Systems (IMBS 96)* part of International Conference on Multi-Agent Systems (ICMAS'96), 1996.

[27] J. Timmis, M. Neal, and J. Hunt, "An artificial immune system for data analysis," *Biosystems*, vol. 55, no. 1-3, pp. 143-150, 2000.

[28] J. Timmis and M. Neal, "A resource limited artificial immune system for data analysis," *Knowledge Based Systems*, vol. 14, no. 3-4, pp. 121-130, June 2001.

[29] L. N. de Castro and F. J. Von Zuben, "aiNet: An artificial immune network for data analysis," Chap. 12 in *Data Mining: A Heuristic Approach*, (Eds. H. A. Abbass, R. A. Sarker, and C. S. Newton), Idea Group, pp. 231-259, 2001.

[30] M. Neal, "An artificial immune system for continuous analysis of timevarying data," *Proc. 1st International Conference on Artificial Immune Systems*. University of Kent at Canterbury, University of Kent at Canterbury Printing Unit, pp. 76-85, September 2002.

[31] A. S. Perelson and G. F. Oster, "Theoretical Studies of Clonal Selection: Minimal Antibody Repertoire Size and Reliability of Self Non-self Discrimination," *Journal of Theoretical Biology*, vol. 81, pp. 645-670, 1979.

[32] J. Carneiro and J. Stewart, "Rethinking "shape space": Evidence from Simulated Docking Suggests that Steric Shape Complementarity is not Limiting for Antibody-Antigen Recognition and Idiotypic Interactions," *Journal of Theoretical Biology*, vol. 169, pp. 391-402, 1994.

[33] T. B. Kepler and A. S. Perelson, "Somatic Hypermutation in B Cells: An Optimal Control Treatment," *Journal of Theoretical Biology*, vol. 164, pp. 37-64, 1993.

[34] A.J. Noest, K. Takumi, and R. de Boer, "Pattern Formation in B-cell Immune Networks: Domains and Dots in Shape-Space," *Physica D*, vol. 105, pp. 285-306, 1997.

[35] J. D. Farmer, N. H. Packard, and A. S. Perelson, "The Immune System, Adaptation, and Machine Learning," *Physica, D*, vol. 22, no. 1-3, pp. 187-204, 1986.

- [36] B. Sulzer, R. J. De Boer, and A. S. Perelson, "Cross-Linking Reconsidered: Binding and Cross-Linking Fields and the Cellular Response," *Biophysical Journal*, vol. 70, pp. 1154-1168, March 1996.
- [37] D. J. Smith, S. Forrest, and A. S. Perelson, "Immunological Memory is Associative," *Proc. International Conference on Multiagent Systems*, Kyoto, Japan, pp. 62-70, 1996.
- [38] R. A. Fisher, "The Use of Multiple Measurements in Taxonomic Problems," *Annals of Eugenics*, vol. 7, pp. 179-188, 1936.
- [39] B. Clarke, E. Fokoué, and H. H. Zhang, *Principles and Theory for Data Mining and Machine Learning*, Springer Series in Statistics, Springer Science+Business Media LLC, 2009.
- [40] C. B. Barber, D. P. Dobkin, and H. T. Huhdanpaa, "The Quickhull algorithm for convex hulls," *ACM Transactions on Mathematical Software*, vol. 22, no. 4, pp. 469-483, Dec 1996, (<http://www.qhull.org>).
- [41] M. Hu, "Visual Pattern Recognition by Moment Invariants," *IRE Transactions on Information Theory*, vol. 8, pp. 179-187, 1962.